Reliable Grasping of Three-Dimensional Untethered Mobile Magnetic Microgripper for Autonomous Pick-and-Place

Jiachen Zhang, Onaizah Onaizah, Kevin Middleton, Lidan You, and Eric Diller

***Abstract*—Manipulation of micrometer to millimeter-scale objects is central to biotechnological and medical applications involving small-scale robotic devices. Mobile untethered microgrippers have been developed, which use magnetic fields for motion and activation of grasping. This letter extends the capabilities of such microgrippers by presenting the first example of reliable and autonomous three-dimensional (3-D) micrograsping and cargo delivery of a microgripper using simple control strategies. This endeavor will allow microgrippers to reliably grasp and transfer microobjects, such as cells, with minimal user input, which is ideal for cooperative tasks performed by multiple microgrippers in future work. The proposed controller autonomously manipulates a 3-D magnetic microgripper for pick-and-place tasks in the 3-D space. By regulating the remotely applied force on the microgripper, the 3-D position and velocity of the microgripper are controlled, and the microgripper grasping, i.e., opening and closing, is determined by the magnetic field strength. In experiments, the microgripper successfully grasps cargoes with cubic, irregular, triangular, and beam shapes using at most 5, 8, 20, and 24 attempts, respectively. The microgripper shown here demonstrates fast grasping due to their complete magnetic actuation method. Moreover, a preliminary cell viability test suggests that the microgripper has no adverse effects on living cells. This study proves the proposed microgripper and controller to be agile and reliable tools for biomedical tasks.**

***Index Terms*—Automation at micro-nano scales, grippers and other end-effectors, soft material robotics.**

I. Introduction

MICROGRIPPERS are precise end-effectors spurred by the demand of high accuracy and delicacy posed by tasks of manipulating microscale objects [1]–[7]. Among the existing microgrippers, the mobile untethered ones become increasingly attractive, because they can move inside small and constrained environments and perform operations that are previously infeasible. With limited sizes, microgrippers usually do not have onboard power or electronics and therefore need to harvest energy from their environments. Magnetic fields are widely used for remote powering and actuation in microrobotics and other areas, e.g. magnetic shape memory alloys [8], since magnetic fields penetrate non-metallic substances and exert both forces and torques on magnetic materials remotely. Moreover, the magnetic fields used for controlling microgrippers have low strength and low frequency and hence are safe for biological organisms. The actuation dexterity and safety of magnetic fields make magnetic microgrippers a suitable tool for biomedical applications [9].

Previously reported mobile microgrippers require additional thermal [1], [2], optical [3], or chemical [4] inputs besides magnetic fields which are used to move the microgrippers. Involving additional mechanisms results in slow operational response, complex multi-modal controllers, and a narrow range of applications due to restrictions on environmental temperature or chemical concentrations. Thus, microgrippers that only require magnetic fields for both motion and grasping could have significant benefits [5]–[7]. Diller *et al.* devised two microgrippers based on magnetic forces and torques, respectively [5]. Out-of-plane assembly is demonstrated by manually teleoperating the microgrippers. However, only the cargoes with mating shapes that match the opening of the microgrippers can be securely picked up. This constraint limits the applicability of the microgrippers. Other existing microgrippers that are fully controlled by magnetic fields are also two-dimensional (2D) in nature and their deformation ranges are small, limiting the cargoes they can grasp. Attacking this limitation, we proposed the first three-dimensional (3D) mobile microgripper that is fully controlled by magnetic fields [10]. The potential of microgrippers in applications depends on their reliability, speed, and capability for parallel operation of multiple microgrippers. Although the manual teleoperation of microgrippers is promising [7], it does not suffice for complex tasks, and therefore the automation of grasping and cargo transport is critical [11]. Control strategies have been developed for magnetic microrobots, including microgrippers, to autonomously manipulate objects [1], [12]. The problem of controlling multiple microrobots for uncoupled behaviours has also been covered [13], [14]. Nonetheless, autonomous grasping

Manuscript received September 10, 2016; revised December 2, 2016; accepted January 5, 2017. Date of publication January 25, 2017; date of current version February 2, 2017. This paper was recommended for publication by Associate Editor H. B. Amor and Editor H. Ding upon evaluation of the reviewers' comments. This work was supported by the Natural Sciences and Engineering Research Council of Canada through the Discovery Grant Program 2014-04703.

J. Zhang, O. Onaizah, and E. Diller are with the Department of Mechanical and Industrial Engineering, University of Toronto, Toronto, ON M5S 3G8, Canada (e-mail: jzhang@mie.utoronto.ca; oonaizah@mie.utoronto.ca; ediller@mie.utoronto.ca).

K. Middleton is with the Institute of Biomaterials and Biomedical Engineering, University of Toronto, Toronto, ON M5S 3G9, Canada (e-mail: kevin.middleton@mail.utoronto.ca).

L. You is with the Department of Mechanical and Industrial Engineering, University of Toronto, Toronto, ON M5S 3G8, Canada, and also with the Institute of Biomaterials and Biomedical Engineering, University of Toronto, Toronto, ON M5S 3G9, Canada (e-mail: youlidan@mie.utoronto.ca).

Color versions of one or more of the figures in this paper are available online at http://ieeexplore.ieee.org.

Digital Object Identifier 10.1109/LRA.2017.2657879

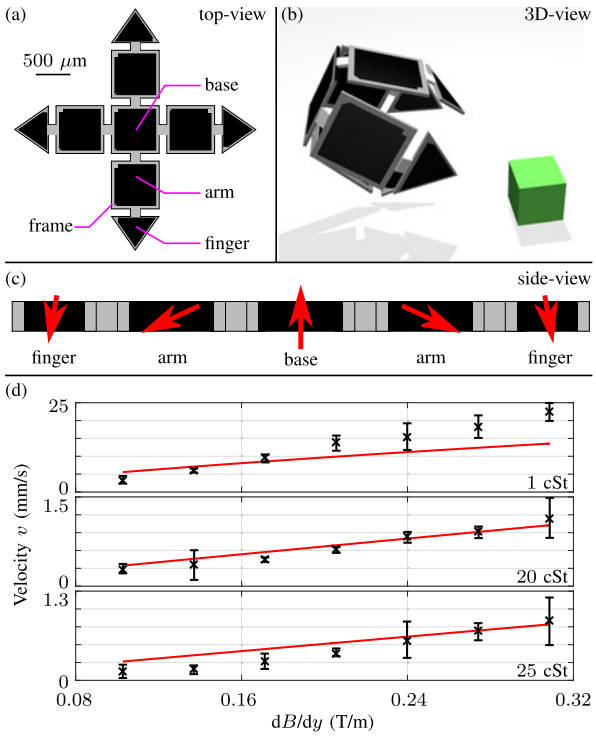

Fig. 1. Microgripper concept and the results of speed characterization. The microgripper is labeled in (a). Moving in liquid, the microgripper grasps cargoes by hugging (power grasping) it (b). The microgripper magnetization is shown by red arrows in (c). The microgripper velocities in different cases are plotted in (d). Black crosses are experimental data and red lines show theoretical predictions. Error bars represent the standard deviation.

and cargo transport using a 3D microgripper with 3D locomotion has not been demonstrated.

For the first time, this paper shows the autonomous 3D micrograsping and cargo delivery of a microgripper using simple controllers and limited feedback. The microgripper position, orientation, and grasping are controlled autonomously and independently. The grasping reliability and versatility of the microgripper are demonstrated and characterized with cargoes of varying geometries and dimensions. The microgripper works with limited feedback, which is a ubiquitous issue in such manipulation tasks. Regulating the magnetic force, the controller can also manipulate the microgripper speed. This work exhibits the efficacy and reliability of the microgripper and its promising potential in robotic and biomedical tasks.

II. Fundamentals of Microgripper

This section revisits the working principles of the microgripper proposed in [10], laying the foundation for the control system. Fabrication of the microgripper are also described.

A. Microgripper Concept

As shown in Fig. 1(a) and (b), the microgripper has a centrosymmetric four-limb structure with one base, four arms, four fingers, and a frame connecting neighboring parts. The microgripper is 3.5 mm long from tip-to-tip and 30 μm thick. It forms an approximate 700 μm cube when fully closed. Although only one single global magnetic field is applied, the three variables of the microgripper, i.e., its shape, orientation, and position, are still controlled independently, because they are related to the strength, direction, and spatiotemporal variance of the applied magnetic field, respectively. Magnetic particles are embedded in the blocks, i.e., the base, arm, and finger parts. Thus, only the blocks experience forces and torques in magnetic fields, receiving energy and control signals. In contrast, the frame does not respond to magnetic fields and is softer than the blocks. Therefore, the blocks function as the 'bones and muscles', providing forces and torques and also the required stiffness to securely grasp cargoes, while the frame works like the 'joints', giving the dexterity of opening and closing reversibly in the 3D space in direct response to the applied field.

An applied magnetic field $\vec{B}$ exerts a force $\vec{f} = \nabla(\vec{m} \cdot \vec{B})$ and a torque $\vec{\tau} = \vec{m} \times \vec{B}$ on a block with a magnetic moment $\vec{m}$. Magnetic torques bend the limbs and close the microgripper. Before the magnetic field is applied, the microgripper is flat and the block magnetic moments neutralize each other, as shown in Fig. 1(c). Defining the magnetization direction of the base as the local positive direction, the microgripper closes when the magnetic field is applied along this direction. On the contrary, the microgripper forms a 'bowl' shape if the magnetic field is in the local negative direction. Since no time-consuming processes, e.g., ambient temperature changes, are involved in the deformation and locomotion, the microgripper can move fast and open and close up to 20 Hz in water [10].

After the microgripper has closed or formed a 'bowl', it exhibits a nonzero net magnetic moment $\vec{m}_{\text{net}}$ along its central axis, which is always aligned with the applied magnetic field. For locomotion, the microgripper can be pulled by the magnetic force on $\vec{m}_{\text{net}}$ in nonuniform magnetic fields. Alternatively, the microgripper can also be rolled by the magnetic torque on $\vec{m}_{\text{net}}$ in rotating magnetic fields.

B. Moving Velocity Versus Field Gradient

When the microgripper is pulled by magnetic forces, a model is proposed to relate the microgripper speed and the applied field gradient, permitting a precise feedback control algorithm. Approximating the closed microgripper as a sphere with a radius $r = 350$ μm, a fluid drag force F_{d} acts on the microgripper and is described by a corrected Stokes' drag model [15] including wall effects from the substrate as

$$F_{\text{d}} = 6\pi\eta r \cdot v \left(1 + \frac{3}{8}\text{Re} + \frac{9}{16}\frac{r}{h}\right), \tag{1}$$

where η is the fluid viscosity and v is the microgripper speed. The gap between the microgripper and the substrate h is assumed to be 30 μm. The net magnetic moment of the microgripper is aligned with the magnetic field gradient, which is along the y-axis of the global 3D coordinate. Thus, a magnetic force F_{m} is generated along the y-axis as

$$F_{\text{m}} = m\frac{\text{d}B}{\text{d}y}. \tag{2}$$

Neglecting the friction, F_{m} balances F_{d} while v is constant. Equaling (1) to (2), the velocity v can be solved. To

experimentally quantify the relationship between the microgripper speed and the field gradient, the microgripper is pulled on a 2D substrate along the y-axis by the forces generated by field gradients. Seven gradient values (from 0.10 to 0.31 T/m) are applied to move the microgripper in liquids with three different viscosity values (1 cSt, 20 cSt, and 25 cSt). Five trials are performed for each configuration and the results are plotted in Fig. 1(d), together with the analytical predictions. The experimental and the predicted data suggest that the microgripper speed is approximately proportional with the field gradient and inversely proportional with the fluid viscosity.

C. Fabrication Procedure of Microgripper

The microgripper is made of polymeric elastomer with embedded permanent magnetic particles through photolithography and replica molding techniques [10]. Negative molds are fabricated for the blocks and the frame using photoresist (SU-8 2025, MicroChem Corp.) on silicon wafers. Magnetic particles (MQFP-15-7, NdPrFeB, Magnequench) are mixed with a polymer (Sylgard 184, Dow Corning) in a 1:1 mass ratio. And the mixture is poured into the block molds for curing. Then the cured blocks are magnetized into the desired magnetization profile using a uniform magnetic field of 1.1 T, and placed into the frame mold. A second kind of polymer (Ecoflex 00-50, Smooth-On), which is highly flexible, fills the frame mold to connect neighboring blocks. The fabrication is complete after the polymer has cured into the frame, then the microgripper is manually harvested from the mold using tweezers. The fabricated microgripper is durable and survives over half a million times of grasping in experiments.

III. Setup and Feedback Controllers

This section presents the setup and the computer vision-based feedback controllers for autonomous pick-and-place.

A. Physical Setup for Control and Actuation

The setup in Fig. 2 includes a coil system with six amplifiers (30A8, Advanced Motion Controls), two cameras (FO134TC, FOculus), an I/O board (Model 826, Sensoray), and custom codes running on a Linux PC. The coils enclose an effective workspace of a 2 cm cube, which is large enough for manipulation tasks within petri dishes. Larger coil systems with open workspaces have been built using the same principles [16]. Currents in the six coils, which are nested along the x, y, and z axes symmetrically, are controlled independently by the input $\mathbf{I} = [i_1, i_2, \cdots, i_6]^{\mathrm{T}}$ and generate a magnetic field $\vec{B}$ at the workspace, which exerts a force $\vec{F}$ and a torque $\vec{\tau}$ on the microgripper. The force $\vec{F}$ varies with the microgripper orientation, which is aligned with $\vec{B}$ by $\vec{\tau}$. In addition, the field strength $|\vec{B}|$ needs to be controlled as it regulates the grasping of the microgripper. Thus, the output of interest is $\mathbf{Y} = [B_x, B_y, B_z, F_x, F_y, F_z]^{\mathrm{T}}$ and is related to the input $\mathbf{I}$ as

$$\mathbf{Y} = \begin{bmatrix} \mathbf{B} \\ \mathbf{F} \end{bmatrix} = \mathbf{A} \cdot \mathbf{I}, \tag{3}$$

where $\mathbf{A}$ is a 6×6 matrix that can be derived from the analysis in [17]. Thus, $\vec{B}$ and $\vec{F}$ are uniquely determined once the input $\mathbf{I}$ is specified. Inversing this relationship, the $\mathbf{I}$ can be obtained for the desired $\vec{B}$ and $\vec{F}$ by

$$\mathbf{I} = \mathbf{A}^{-1} \cdot \mathbf{Y}. \tag{4}$$

It should be noted that the coil system used in this study is not designed to generate magnetic forces. The fact that the coil system only has six coils in a symmetric configuration leads to singularities in (4), meaning that some combinations of $\vec{B}$ and $\vec{F}$ cannot be achieved. In addition, the amplifiers only work at currents up to 19 A. Alternatively, approximate forces can be applied on the microgripper without solving (4). The three pairs of coils are along the x, y and z axes, respectively. Uniform field is generated in the workspace when the two coils in the same pair run currents with the same amplitude and direction. Otherwise, the resultant magnetic field is nonuniform and magnetic forces will be exerted on the microgripper (Fig. 2(c)). Forces generated using this method are approximations because the coupling of the six coils and the microgripper orientation are not considered. Nevertheless, this method allows the user to control the range of the input current $\mathbf{I}$ and avoid extensive computations, and is therefore used as an alternative in the proposed controller.

B. Feedback Control System

The microgripper 3D position is changed by applying either nonuniform magnetic fields to exert forces on the microgripper or rotating fields to roll the microgripper on surfaces. Controlling the position is nontrivial, and thus a high-level director is designed for this task together with two low-level controllers, including a proportional (P) controller and a two-point (on-off) controller. The structure of the control system is illustrated in Fig. 3. The P controller regulates both the direction and the amplitude of the force on the microgripper, while the two-point controller only manages the force direction.

The two low-level controllers take the goal position and the grasping level as inputs while output a binary signal of 'success' or 'failure'. The goal position contains three coordinate values in the 3D workspace frame and is determined by the cargo position (before grasping) or the cargo destination (after grasping). The grasping level $\zeta \in [0, 1]$ decides the microgripper shape and the grasping action: the microgripper is fully open when $\zeta = 0$ and fully closed when $\zeta = 1$. In this work, ζ is either 0 or 1. Camera frames are processed as in Fig. 2(b) to track the microgripper position in real time: The x and y coordinates are obtained from the blurred and binarized top-view frame using a contour finding algorithm, while the side-view frame is subtracted from a reference background, blurred, and binarized to show the z coordinate. The controller monitors the microgripper position, builds a vector pointing from the microgripper to its goal, computes the corresponding currents for each coil using the selected low-level controller, and then outputs the calculated currents to the coil system.

The P controller regulates the applied magnetic force on the microgripper to position it in the 3D space: The desired force is determined proportionally based on the distance from the

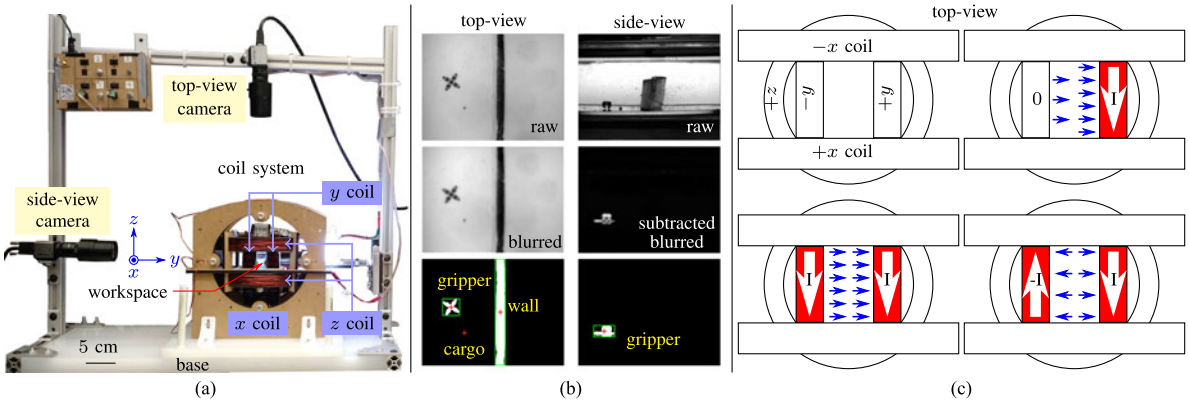

Fig. 2. Experimental setup, image processing process, and coil schematics. The setup is shown in (a) with annotations. Power suppliers, current amplifiers, and the computer are not shown here for better visualization. As shown in (b), frames from the top-view and side-view cameras are processed to extract the centroids of the microgripper and the cargo. The working principles of the coil system is depicted in (c). Magnetic field is generated in the workspace when one or more coils are powered. The resultant magnetic field is uniform only when the currents in the same coil pair have identical amplitude and direction. All other configurations lead to nonuniform field and nonzero field gradient. Coils with current are marked as red and the density of blue arrows denotes the resultant field strength.

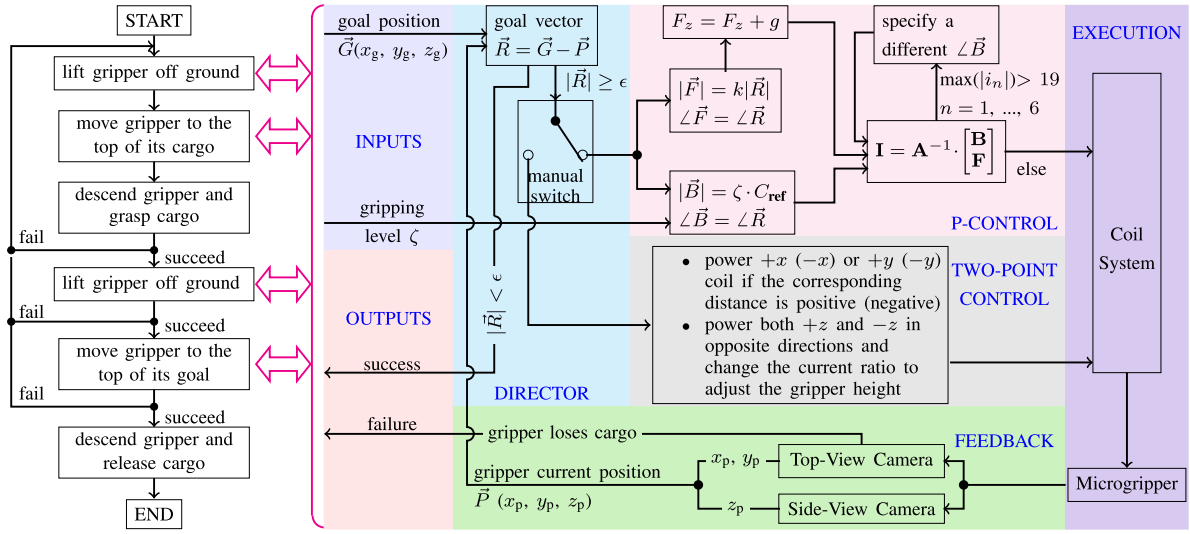

Fig. 3. Flow chart and block diagram of the feedback controller system for autonomous pick-and-place tasks. The microgripper 3D position is controlled based on the logic shown in the block diagram. One of the two low-level controllers, i.e., a P controller and a two-point controller, is enabled based on whether or not the magnetic force needs to be accurately regulated.

microgripper to its goal, with an offset to compensate its own weight. The parameter of the P controller is obtained from trial-and-error. The microgripper is specified to point towards its goal, and the required current set $\mathbf{I}$ is calculated using (4). When magnetic actuation singularities are encountered or the calculated $\mathbf{I}$ exceeds the amplifier limit, a slightly different microgripper orientation is specified to retry (4) until a feasible $\mathbf{I}$ is obtained. In most cases, a feasible $\mathbf{I}$ can only be obtained after several trials, because the amplifier has a limited current range and no constraint is imposed on the calculation of (4). The repeated calculations of (4) make the P controller much more computationally expensive than the two-point controller. Thus, the manual switch in Fig. 3 is configured to the P controller only when the force amplitude needs to be controlled. Otherwise, the simpler two-point controller is selected. Powering the coil system with the obtained $\mathbf{I}$, the desired 3D force will be applied on the microgripper. The alternative low-level controller is a two-point controller. The x-y position of the microgripper is altered by powering selected coils in the x and y coil pairs. To adjust the microgripper height (z coordinate), the $+z$ and $-z$ coils are powered with currents in opposite directions to generate a strong enough magnetic force to overcome the microgripper weight.

With the control over the microgripper position, a high-level director plans the paths and actions of the microgripper during pick-and-place tasks. Note that the controller only requires two cameras that track the centroids of the microgripper and the cargo, making the controller easier to implement than other ones that require precise and complicated feedback. This paper focuses on demonstrating the capabilities of the proposed microgripper with simple control strategies and limited feedback. Considering that the integral (I) and the derivative (D) components of a PID controller are mainly used to minimize the steady-state error and the overshoot, respectively, using a PID in this work does not promise much performance benefits because the microgripper are doing waypoint-following instead of path-following tasks. The detailed investigations of controller

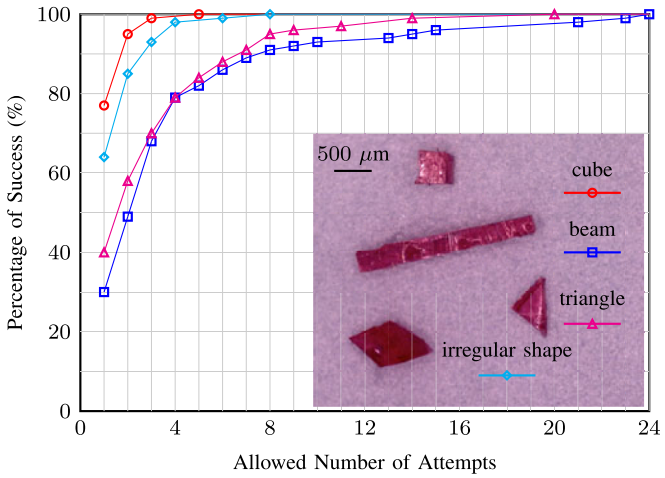

Fig. 4. Results of the grasping characterization of the microgripper with different cargoes. A photograph of the cargoes are shown as the inset.

TABLE I
ANALYSIS OF THE GRASPING CHARACTERIZATION RESULTS

Cargo Shape	No. of Attempt in One Grasping (avg. ± std.)	Time of Each Attempt (avg. ± std. second)	Success Probability (%)
cube	1.30 ± 0.64	0.745 ± 0.035	76.9
irregular	1.64 ± 1.15	0.773 ± 0.042	61.0
triangle	3.18 ± 3.21	0.765 ± 0.043	31.4
beam	3.95 ± 4.65	0.780 ± 0.048	25.3

parameter optimization, stability, and comparison with other controllers are beyond the scope of this paper and will be addressed in future research.

IV. EXPERIMENTS AND RESULTS

In this section, the microgripper performs autonomous 3D pick-and-place tasks and grasps different cargoes. Results of the cell viability test of the microgripper are also presented.

A. Reliable Grasping Characterization

The grasping reliability is investigated with four cargoes made of polymer (Sylgard 184, Dow Corning) in different shapes (cube, triangular plate, beam, and irregular shape) (Fig. 4). In each trial, the two-point controller manipulates the microgripper in distilled water to keep attempting to grasp a cargo and lift it up until it succeeds. Fig. 4 shows the results of 100 consecutive trials for each cargo. Being more rounded, the cube and the irregular cargo fit into the microgripper regardless of their poses and therefore are easier to be picked up. In contrast, the triangular plate is thin and can easily escape the grasping no matter what its orientation is. The beam is the most difficult one, because it is longer than the microgripper limbs and the microgripper can only grasp a portion of it.

Table I shows that the average number of attempts to pick up a cargo is less than 4 for all cargoes, demonstrating the microgripper versatility that originates from its 3D structure and power grasping behavior. Since only the positions of the microgripper and the cargo are tracked, confusion arises in the algorithm when the microgripper visually occludes the cargo. A more comprehensive feedback should settle this confusion and also provide the orientation information of the microgripper and the cargo, thus reducing the number of attempts required for successfully grasping a cargo. Table I suggests one attempt takes about 0.8 second, starting when the microgripper begins to descend and ending after the microgripper has fully closed. The grasping is intentionally slowed down to prevent the microgripper from blowing the cargo away. If its speed is not limited, the microgripper can close within 25 ms in water using this electromagnetic coil [10]. And the microgripper can deform even faster in a stronger magnetic field. Note that the fluid viscosity also affects the time of each attempt.

B. 3D Autonomous Pick-And-Place

The microgripper is maneuvered to perform 3D autonomous pick-and-place tasks. The microgripper picks up a cargo lying on the substrate, carries it over a wall, and delivers it to the other compartment of the workspace. In this process, the controller tracks the microgripper and the cargo, plans a path towards the goal that goes over the wall, detects whether or not the microgripper has successfully grasped its cargo, and monitors if the microgripper loses its cargo in transportation.

The P controller is used when the force amplitude on the microgripper needs to be regulated. To prevent the amplifiers from overheating, currents are applied with a 0.05 second interval between every 0.3 second. Silicone oil (20 cSt viscosity at 25 °C) is used as the media to slow down the microgripper, allowing the intermediate magnetic field to work. Note that if fluids with different viscosities or densities are used, the interval time needs to be adjusted. Frames are shown in Fig. 5(a)–(f) with the 3D path of the microgripper in Fig. 5(h). The microgripper points downwards when it descends to its cargo and changes its orientation to upwards after grasping, after which, the microgripper opens to allow the cargo to fall into its hug and re-grasps the cargo (Fig. 5(g)). The upwards orientation secures the cargo transportation. When the force amplitude on the microgripper is unimportant, the two-point controller is utilized. Since the $\mathbf{I}$ is directly specified instead of being calculated from (4), its current amplitude can be easily limited. Therefore, the magnetic field is always applied and water is used instead of silicone oil to increase the operation speed. In this case, the execution time is shorter than the one required by the P controller: 16 versus 74 seconds. The microgripper path in this experiment is shown in Fig. 5(i).

The results endorse the 3D locomotion capability of the microgripper and the efficacy of the proposed controller. Without being limited to the 2D plane, the microgripper can move to the top of the cargo, and then descend to grasp the cargo vertically, without disturbing the planar environment around the cargo, which potentially contains other microobjects.

C. Bio-Compatibility Test

Results of a preliminary bio-compatibility test suggest that the microgripper does not leach toxic particles and the cells

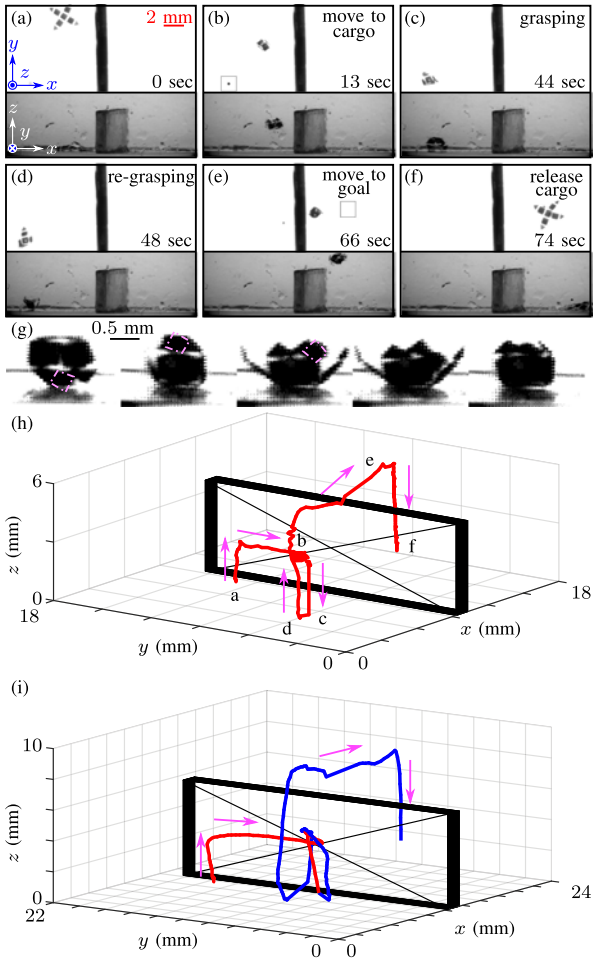

Fig. 5. Results of the autonomous 3D pick-and-place experiments. Top- and side-views of the workspace are shown chronologically in (a)–(f). The process of re-grasping is shown in (g) with the cargo marked out by a dashed square. The microgripper position in experiments with the P controller and the two-point controller are shown in (h) and (i), respectively. Corresponding positions of the frames in (a)–(f) are labeled in (h) by their indexes. Red line represents the first grasping attempt, while the blue line stands for the second attempt.

in direct contact with the microgripper could develop normal functions after being released. Thus, the microgripper could be suitable for biomedical applications with further study. More details of the test are included in the supplementary material.

V. Conclusion

This paper demonstrates the reliable and versatile grasping of the proposed microgripper using simple control strategies and limited feedback information. Autonomous 3D micrograsping and cargo delivery are presented and characterized for the first time. With the 3D locomotion capability, the microgripper can pick up a cargo from a substrate without disturbing its surrounding planar environment, which is beneficial in manipulating cells inside a population. Even with limited optical feedback due to visual occlusions, the microgripper still successfully grasps all cargoes tested, when multiple attempts are allowed. The results suggest that the micrograsping and the cargo delivery using autonomous magnetic microgrippers are versatile, reliable and agile. This paper shows that the proposed microgripper has a promising potential in manipulating microobjects, e.g., cells, in remote confined environments, such as microfluidic channels for biomedical applications. Future studies will examine the microgripper in biomedical tasks such as biopsy, cell manipulation, and targeted drug delivery. Microgripper miniaturization will be investigated to satisfy the corresponding size requirements, and autonomous manipulation using a team of mobile microgrippers will be studied to increase the throughput and efficiency.

References

[1] F. Ongaro *et al.*, "Control of untethered soft grippers for pick-And-place tasks," in *Proc. 6th IEEE RAS/EMBS Int. Conf. Biomed. Robot. Biomechatronics*, 2016, pp. 299–304.

[2] J. Breger *et al.*, "Self-folding thermo-magnetically responsive soft microgrippers," *ACS Appl. Mater. Interfaces*, vol. 7, no. 5, pp. 3398–3405, 2015.

[3] S. Fusco *et al.*, "Self-folding mobile microrobots for biomedical applications," in *Proc. IEEE Int. Conf. Robot. Autom.*, Hong Kong, 2014, pp. 3777–3782.

[4] J. Randhawa, T. Leong, N. Bassik, B. Benson, M. Jochmans, and D. Gracias, "Pick-and-place using chemically actuated microgrippers," *J. Amer. Chem. Soc.*, vol. 130, no. 51, pp. 17 238–17 239, 2008.

[5] E. Diller and M. Sitti, "Three-dimensional programmable assembly by untethered magnetic robotic micro-grippers," *Adv. Funct. Mater.*, vol. 24, pp. 4397–4404, 2014.

[6] J.-C. Kuo, H.-W. Huang, S.-W. Tung, and Y.-J. Yang, "A hydrogel-based intravascular microgripper manipulated using magnetic fields," *Sensors Actuator A, Physical*, vol. 211, pp. 121–130, 2014.

[7] S. Chung, X. Dong, and M. Sitti, "Three-dimensional heterogeneous assembly of coded microgels using an untethered mobile microgripper," *Lab Chip*, vol. 15, no. 7, pp. 1667–1676, 2015.

[8] J.-Y. Gauthier, C. Lexcellent, A. Hubert, J. Abadie, and N. Chaillet, "Magneto-thermo-mechanical modeling of a magnetic shape memory alloy Ni-Mn-Ga single crystal," *Ann. Solid Struct. Mech.*, vol. 2, no. 1, pp. 19–31, 2011.

[9] E. Diller and M. Sitti, "Micro-scale mobile robotics," *Found. Trends Robot.*, vol. 2, no. 3, pp. 143–259, 2011.

[10] J. Zhang and E. Diller, "Tetherless mobile micrograsping using a magnetic elastic composite material," *Smart Mater. Struct.*, vol. 25, no. 11, 2016, Art. no. 11LT03.

[11] M. Sitti *et al.*, "Biomedical applications of untethered mobile milli/microrobots," *Proc. IEEE*, vol. 103, no. 2, pp. 205–224, Feb. 2015.

[12] F. Ongaro *et al.*, "Autonomous planning and control of soft untethered grippers in unstructured environments," *J. Micro-Bio Robot.*, no. 1, pp. 1–9, 2016.

[13] A. Becker, Y. Ou, P. Kim, M. Kim, and A. Julius, "Feedback control of many magnetized: Tetrahymena pyriformis cells by exploiting phase inhomogeneity," in *Proc. IEEE/RSJ Int. Conf. Intell. Robots Syst.*, 2013, pp. 3317–3323.

[14] A. Mahoney, N. Nelson, K. Peyer, B. Nelson, and J. Abbott, "Behavior of rotating magnetic microrobots above the step-out frequency with application to control of multi-microrobot systems," *Appl. Phys. Lett.*, vol. 104, 2014, Art. no. 144101.

[15] P. Vasseur and R. Cox, "The lateral migration of spherical particles sedimenting in a stagnant bounded fluid," *J. Fluid Mech.*, vol. 80, no. 3, pp. 561–591, 1977.

[16] B. Kratochvil *et al.*, "MiniMag: A hemispherical electromagnetic system for 5-DOF wireless micromanipulation," in *Experimental Robotics*, O. Khatib, V. Kumar, and G. Sukhatme, Eds.Berlin, Germany: Springer-Verlag, 2014, pp. 317–329.

[17] A. Petruska and B. Nelson, "Minimum bounds on the number of electromagnets required for remote magnetic manipulation," *IEEE Trans. Robot.*, vol. 31, no. 3, pp. 714–722, Jun. 2015.